



**Hydrogen evolution reaction (HER) on Au@Ag
ultrananoclusters as electro-catalysts**

Journal:	<i>Nanoscale</i>
Manuscript ID	NR-ART-07-2018-006105
Article Type:	Paper
Date Submitted by the Author:	29-Jul-2018
Complete List of Authors:	Chang, Le; Beijing University of Chemical Technology, Department of chemical engineering Cheng, Daojian; Beijing University of Chemical Technology, Department of chemical engineering Sementa, Luca; Istituto per i Processi Chimico-Fisici Consiglio Nazionale delle Ricerche, Fortunelli, Alessandro; Consiglio Nazionale delle Ricerche, ICCOM

Hydrogen evolution reaction (HER) on Au@Ag ultranano-clusters as electro-catalysts

Le Chang,¹ Daojian Cheng,^{1,*} Luca Sementa,² Alessandro Fortunelli^{2,*}

¹ Beijing Key Laboratory of Energy Environmental Catalysis, State Key Laboratory of Organic-Inorganic Composites, Beijing University of Chemical Technology, 100029, Beijing, China

² CNR-ICCOM & IPCF, Consiglio Nazionale delle Ricerche, via Giuseppe Moruzzi 1, 56124, Pisa, Italy

Abstract

We propose and investigate computationally Ag-Au subnanometer clusters as catalysts for the hydrogen evolution reaction (HER). Focusing on Ag₁₂Au, we conduct a complete first-principles study of the HER process on this Au@Ag ultranano-catalyst. After determining the hydrogen-saturated resting state under standard conditions as Ag₁₂AuH₁₁, HER reaction energies and barriers are predicted also including solvent effects using both implicit and explicit models. We find that Ag₁₂Au is a good candidate as HER catalyst, with a good stability and an overall reaction energy barrier 0.89 eV as an upper bound. We also draw indications for the design of HER subnanometer catalysts.

*corresponding authors email: chengdj@mail.buct.edu.cn, alessandro.fortunelli@cnr.it

INTRODUCTION

In the context of the increasing global energy demand, the exploitation of renewable and clean energies represents one of the greatest scientific challenges^{1,2}. In this context, hydrogen (H₂) is regarded as an appealing energy carrier, alternative to carbon-containing compounds, suitable to store energy durably for further use^{3,4}. Hydrogen can be generated by water splitting electrochemically at the cathode in a process known as hydrogen evolution reaction (HER) while oxygen is evolved at the anode in the oxygen evolution reaction (OER)^{5,6}, thus converting electricity into a stable form of chemical energy. Electrocatalyst materials are the key enabling technology for these processes, and their rational design is of crucial importance for the efficiency of H₂ and O₂ production. Although the most popular electro-catalysts for HER are based on platinum (Pt)⁷, its high cost and global scarcity have promoted efforts to develop alternative catalysts⁸⁻¹¹. For instance, various earth-abundant transition metals (Fe, Co, Ni, Mo) and their mixtures (e.g. NiMo, NiFe¹²⁻¹⁴) have been designed as efficient HER electro-catalysts under either acidic or alkaline conditions^{15,16}. Other studies have proposed molecular-like thiolate-protected metal clusters, such as PtAu₂₄(SR)₁₈, with promising results¹⁷. Transition-metal sulfides, phosphides, selenides, borides, carbides, and nitrides have also recently attracted great interest in this field⁸⁻¹⁸.

Here we propose and explore via computational tools a novel class of materials as HER electro-catalysts: bimetallic silver@gold subnanometer (or ultranano) clusters. Several reasons justify this choice. Thanks to their high surface area, high activity, and size-tunable electronic properties, silver and gold nanoparticles have been the focus of intense attention in several fields such as catalysts, sensors, etc.¹⁹⁻²² including HER^{23,24}. Moreover, mixed Ag-Au systems have been proved to exhibit enhanced chemical stability in addition to specific superior features compared to pure Au or Ag nanoparticles, such as for example the plasmonic response of Au@Ag core-shell nanospheres²⁵. Bimetallic Ag-Au clusters also exhibit favorable electronic properties, which could make them appropriate as receptors of electrons and H₃O⁺ water-ions to produce gaseous H₂ efficiently²⁶. Our choice was also inspired²⁷ by recent work showing that Ag clusters grown on Au nanorods enhance energy harvesting and increase stability in light-induced HER catalysts²⁸, but, at variance with this previous study, the absence of the plasmon resonance at the ultrananoscale suggested us to exclude optical phenomena. Finally, after completion of this work, alloyed Cu-Pt dual sites on Pd nanorings were demonstrated to possess a very high HER activity²⁹, which further supports this line of investigation, i.e., metal ultrananoclusters as HER catalysts. In designing potential candidates we took into account the known strong dependence of catalytic activity on the exact number of Ag atoms in the ultrananocluster, as e.g. observed in the effect on storage properties in lithium–oxygen batteries³⁰. We thus chose to investigate Au@Ag clusters in the Ag-rich régime, specifically the Ag₁₂Au cluster, as electrochemical catalyst for HER. Due to their ultra-small size and thus high active surface area, their near-metallic character, and the high content in Ag (less expensive than Au or Pt), these systems could combine a reasonably lost cost, good conducting properties, and good efficiency, which may pave the way for further investigations combining optical and electrical phenomena. Our goal here is then a complete investigation via first-principles simulations of a Au@Ag ultrananocluster at a selected composition as HER catalyst, to unveil the detailed mechanistic steps of the HER process on these systems, hence drawing insight and if possible general principles

that can trigger the development and rational design of HER cluster catalysts³¹.

The article is organized as follows. In Section 2 we describe our methodology. Results are presented and discussed in Section 3, while Section 4 summarizes our main conclusions.

2. THEORETICAL METHOD

In Section 2.1 we provide computational details of the present simulations, while in Section 2.2 we describe the approach employed to model the HER process on Ag-Au nanoclusters.

2.1 Computational Details

Density-functional theory (DFT) calculations on Ag₁₂AuH_m systems were performed using the Quantum Espresso (QE) package³² and ultra-soft pseudopotentials. A semi-empirical correction (Grimme-D2)³³ was added to the Perdew-Burke-Ernzerhof (PBE) exchange-correlation (xc-)functional³⁴ to account for dispersion interactions^{35,36}. A cubic unit cell measuring 38 Å in side length, and 40 Ry and 400 Ry as the cutoffs for the plane-wave representation of the wave function and the density, respectively, were employed. Calculations were performed spin-restricted for even-electron (closed-shell) systems and spin-unrestricted for odd-electron systems, at the Gamma point only. The cell size was determined from calculations on charged Ag₁₂AuH_m species: cells of dimension 30 Å or 38 Å in length were considered, finding that the total energy of the Ag₁₂AuH₁₁ anion is lower by 0.29 eV for a cell size of 38 Å with respect to a cell size of 30 Å, but that the energy does not change significantly for cell sizes larger than 38 Å. The electronic affinity (EA) of Ag₁₂AuH₁₁ in the gas-phase is determined as 2.545 eV, while that of Ag₁₂AuH₁₂ is 3.484 eV. Solvation energies (*E_s*) of the charged species in water were estimated both via explicit solvent simulations and via an implicit-solvent polarizable continuum model using the Born formula as:

$$E_s = -\frac{1}{2} \frac{q^2}{R} \quad (1)$$

where *q* is the charge and *R* is the radius of the cluster. In our case, *R* is estimated as 13.89 a.u. for both clusters and *q* is 1, therefore *E_s* = 0.980 eV. The electronic affinity of Ag₁₂AuH₁₁ and Ag₁₂AuH₁₂ clusters in water thus increase to 3.525 and 4.464 eV, respectively.

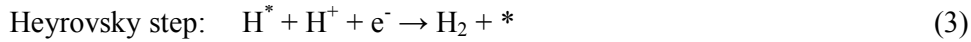
Energy barriers for selected reactive processes were calculated using QE and the Nudged Elastic Band (NEB) method³⁷⁻³⁹. In this approach, the minimal energy path between two stable molecular conformations is sought by optimizing the energy of a set of intermediate replicas that represent the gradual transition between end points and that are connected by harmonic springs. Here, we employed 4 intermediate replicas, with the reference optimized structure and the result of the unconstrained optimizations as starting and end points, respectively.

Selected DFT geometry optimizations and ab initio Molecular Dynamics (AIMD) simulations were conducted using the CP2K package⁴⁰ whose DFT algorithms are based on a hybrid Gaussian/Plane-Wave scheme (GPW)⁴¹. Pseudopotentials derived by Goedecker, Teter, and Hutter (GTH)⁴² were chosen to describe the core electrons of all atoms and DZVP basis sets⁴³ to represent the DFT Kohn-Sham orbitals. The semiempirical Grimme-D3³³ correction was added to the PBE xc-functional³⁴ to take

into account dispersion interactions. The cutoff for the auxiliary plane-wave representation of the density was 300 Ry. AIMD simulations were performed both to test the stability of $\text{Ag}_{12}\text{AuH}_m$ species and introduce thermal effects, and to model the HER Volmer step (see below) using an explicit solvent. AIMD runs were carried out ranging from 300 to 600K and 1 atm pressure. The temperature was controlled using a Nose–Hoover thermostat. A time step of 0.5 femtosec was used to integrate the equations of motion. A trajectory of 10 picosec was typically generated and used for analysis. This time scale is comparable with the reported time scale for the simulation of Au nanoclusters which has been validated in previous work^{44, 45}. For the free cluster, a simulation box with cell size of 38 Å nm in each Cartesian direction was employed, large enough to make cluster/cluster interactions negligible (see above). For the explicitly solvated clusters, a simulation box with 100 explicit water molecules embedding the $\text{Ag}_{12}\text{AuH}_{11}$ or $\text{Ag}_{12}\text{AuH}_{12}$ clusters was employed, together with identical AIMD simulation numerical parameters (time step, total simulation time, thermostat).

2.2 Theoretical Approach to HER

In electrochemistry, HER is a classic example of a two-electron transfer reaction with one catalytic intermediate, H^* (where * denotes a site on the electrode/catalyst surface), and in acidic conditions is assumed to occur via the Volmer-Heyrovsky mechanism⁴⁶:



The overall rate of the reaction via this Volmer-Heyrovsky mechanism is determined by the adsorption free energy of this hydrogen intermediate, H^* , which should be neither too strong (which would hinder H_2 desorption in the Heyrovsky step) nor too weak (otherwise, H adsorption in the Volmer step would be slow). The HER rate as a function of hydrogen adsorption energy should thus follow a volcano plot, according to the Volmer-Heyrovsky and Volmer-Tafel routes to designing optimal catalysts⁴⁷⁻⁵⁰.

We model the HER hydrogen adsorption-reduction-desorption processes and evaluate reaction free-energy diagrams on the electrode surface by combining DFT and gas-phase free energies. In particular, the Gibbs free energy of $[\text{H}^+ + \text{e}^-]$, $G_{\text{H}^+ + \text{e}^-}$, is calculated as one-half of the Gibbs free energy of gas-phase H_2 :

$$G_{\text{H}^+ + \text{e}^-} = \frac{1}{2}G_{\text{H}_2} ; \quad G_{\text{H}_2} = G_{\text{trans}} + G_{\text{vib}} + G_{\text{rot}} + G_{\text{ele}} \quad (4)$$

where G_{trans} , G_{vib} , G_{rot} , and G_{ele} are the translational, vibrational, rotational and electronic energy terms, and the first three terms can be derived from the partition function of gas-phase H_2 , while G_{ele} is obtained by DFT relaxation of the H_2 molecule. In detail, under standard conditions (room temperature = 298 K, H_2 pressure = 1 atm) in our approach G_{ele} is -31.718 eV; $G_{\text{rot}} + G_{\text{trans}} = -0.29$ eV ; and G_{vib} is neglected due to the cancellation of vibrational terms between gas-phase and adsorbed species. We thus obtain $G_{\text{H}^+ + \text{e}^-} = \frac{1}{2}G_{\text{H}_2} = -16.004$ eV under standard conditions.

Moreover, as customary in the literature^{48, 51-53} we exploit the fact that at zero bias (bias = 0. V) on the electrode there is equilibrium between hydronium ion plus an electron from the electrode, and gas-phase H₂:



to equate the free energy of the pair (hydronium plus electron) with one-half of the free energy of gas-phase H₂ at zero bias, then properly shifting this quantity at a generic bias V^{48, 51-53}.

Finally, we need the energy of an electron separately to estimate energy differences upon electron exchange between the electrode and the Ag₁₂AuH_m catalysts. The work function of the Pt electrode at zero charge is 6.167 eV, which decreases in a water environment to 5.167 eV^{54, 55}. Assuming that the HER reaction occurs at -0.9 V bias, the work function (WF) of Pt electrode, i.e., the chemical potential of the electron in Eq.(2), is thus calculated under these conditions as 4.267 eV.

3. RESULTS AND DISCUSSIONS

Inspired by the HER experiments²⁸ of Ag clusters growing on Au nanorods, we choose a Ag₁₂Au icosahedral cluster of 13 atoms as the model on which to investigate HER. This Au@Ag cluster corresponds to the smallest structurally magic cluster with icosahedral symmetry, its size is small enough to allow us to conduct a systematic first-principles investigation, but is also large and thus stable enough to accommodate a significant number of H adatoms without disruption of the cluster⁵⁶. Although Au tends to occupy surface sites in bare Ag-Au nanoclusters⁵⁷, here we focus on a Au(core)-Ag(shell) arrangement to mimic the exohedral arrangement of Ag clusters in experiment²⁸. Importantly, as we will see below, the catalytically species at high hydrogen coverage is in fact Ag₁₂AuH₁₁, and at this coverage the configuration with Au in the core (which we focus on) is only 0.082 eV higher in energy with respect to the configuration with Au in a surface site. The Au(core)@Ag(surface)₁₂H₁₁ configuration that we investigate is associated with a minor energy penalty, is significantly populated under standard conditions, and is thus a realistic model on which to study HER.

3.1 Hydrogen saturation and resting state of the catalyst

The first step in a computational study of on ultrananoclusters is to determine the resting state of the catalyst under reaction conditions^{58, 59}. The adsorption of a single H atom onto Ag₁₂Au at its three main surface adsorption sites: bridge, hollow, and top sites, followed by full relaxation of the structures shows that adsorption strengths are in the order: bridge (-2.457 eV) \approx hollow (-2.457 eV) < top (-2.161 eV), in agreement with previous studies (see e.g. Ref.⁶⁰ and references therein). Such a preference for bridge or hollow adsorption sites is however attenuated at higher hydrogen coverage. For example, the energy difference between hydrogen adsorption on 12 bridge and 12 top sites is only \approx 0.086 eV/H-atom. Moreover, the Ag₁₂Au cluster quickly reaches saturation: when more than 13 H atoms are placed around the cluster surface, free H₂ molecules evolve during the geometry relaxation step (this doesn't occur up to 13 adsorbed hydrogens). Although H adsorption on bimetallic nanoparticles has been studied in previous work⁶⁰⁻⁶⁴, saturation has rarely been considered, with few exceptions⁶⁵. Finally, a crucial point to consider is that hydrogen adsorption energies on

these ultrananostructures exhibit an odd/even alternation (i.e., they are larger on average by $\approx 0.5\text{-}0.7$ eV for odd number of hydrogens with respect to even number), due to the fact that the Ag_{12}Au cluster possesses one unpaired electron and needs an odd number of H atoms to realize an (energetically more stable) closed shell configuration.

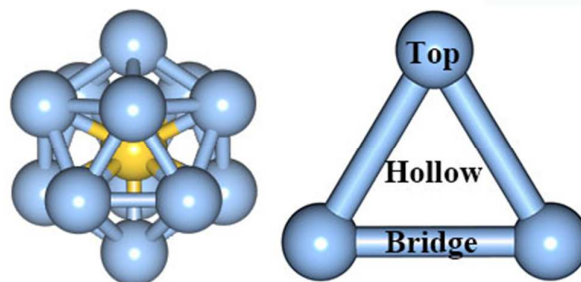


Figure 1. Adsorption sites of H atoms on the icosahedral structure of the Ag_{12}Au cluster: bridge, top, and hollow, respectively. Ag and Au atoms are represented by light blue and yellow spheres, respectively.

Geometry relaxations have then been performed on the $\text{Ag}_{12}\text{AuH}_m$ clusters (with $m=1, 3, 5, 7, 9, 11, 12, 13$) clusters. From the structural point of view, a quasi icosahedral arrangement (see Figure 1) is essentially kept up to 7 adsorbed H atoms, whereas adsorption of 9 H atoms or more changes the symmetry of the cluster and restructures it as shown in Figure 2 for $\text{Ag}_{12}\text{AuH}_m$ with $m=11\text{-}13$.

The main results of such calculations is that the resting state of the system under standard thermodynamic conditions is $\text{Ag}_{12}\text{AuH}_{11}$ with very minor admixtures of $\text{Ag}_{12}\text{AuH}_9$ and $\text{Ag}_{12}\text{AuH}_{13}$. Indeed, we find:

$$G(\text{Ag}_{12}\text{AuH}_{11}) - G(\text{Ag}_{12}\text{AuH}_9) - G(\text{H}_2) < 0 ; \quad \Delta G = -0.130 \text{ eV} \quad (1)$$

$$G(\text{Ag}_{12}\text{AuH}_{13}) - G(\text{Ag}_{12}\text{AuH}_{11}) - G(\text{H}_2) > 0 ; \quad \Delta G = +0.168 \text{ eV} \quad (2)$$

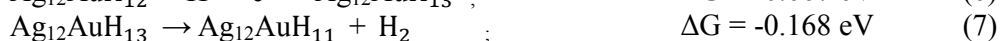
where $G(\text{H}_2)$ is the Gibbs free energy of H_2 obtained as described in Section 2.2. To further support this result and to check the stability of the $\text{Ag}_{12}\text{AuH}_{11}$ and $\text{Ag}_{12}\text{AuH}_{13}$ species, AIMD simulations on $\text{Ag}_{12}\text{AuH}_{11}$ were performed at 300, 350, 400, 450, 500, 550, and 600 K, each AIMD simulation starting from the end-point of the previous one and lasting 10 picosec. The structure of the $\text{Ag}_{12}\text{AuH}_{11}$ cluster remained basically unchanged after the AIMD runs, and a final local optimization produced a configuration identical to the initial configuration shown in Figure 2. On the opposite, an AIMD simulation on $\text{Ag}_{12}\text{AuH}_{13}$ performed at 400 K showed that the system spontaneously produced $[\text{Ag}_{12}\text{AuH}_{11} + \text{H}_2]$ before the end of the 10-picosec run: this means that $\text{Ag}_{12}\text{AuH}_{13}$ is higher in free energy and spontaneously transforms into $\text{Ag}_{12}\text{AuH}_{11} + \text{H}_2$, at 400 K, in good agreement with the energetics reported in Eq. (2). We thus assume $\text{Ag}_{12}\text{AuH}_{11}$ as the resting state of our system under realistic (standard) conditions.

3.2 HER catalytic steps

After determining the hydrogen saturation level and the lowest-energy geometry of $\text{Ag}_{12}\text{AuH}_{11}$, we explored HER mechanistic steps on this cluster in the super-saturation régime, via both implicit-solvent (3.2.a) and explicit-solvent (3.2.b)

models.

Following the super-saturation path, the first point is to determine the quantum-mechanical (QM) energy difference (ΔE) between neutral clusters in their lowest-energy geometry with increasing H content, for which we obtain: $\Delta E(\text{Ag}_{12}\text{AuH}_{11} \rightarrow \text{Ag}_{12}\text{AuH}_{12}) = -15.168 \text{ eV}$, $\Delta E(\text{Ag}_{12}\text{AuH}_{12} \rightarrow \text{Ag}_{12}\text{AuH}_{13}) = -16.671 \text{ eV}$. These numbers are consistent with the even/odd alternation principle, and it can be noted that their average is -15.919 eV which is not sufficient to overcome the free energy of $\frac{1}{2} \text{H}_2$ (equal to -16.004 eV under standard conditions, as estimated in Section 2.2). According to the Volmer-Heyrovsky route⁴⁶, we assume that HER on the Ag_{12}Au cluster catalysts via a super-saturation path proceeds via the following steps, whose energetics can be derived from the QM values above and is also reported:



where, as discussed in Section 2.2, the free energy of $[\text{H}^+ + \text{e}^-]$ is taken as half that of $G(\text{H}_2)$ under standard conditions at zero bias, -16.004 eV at bias = 0.0 Volt.

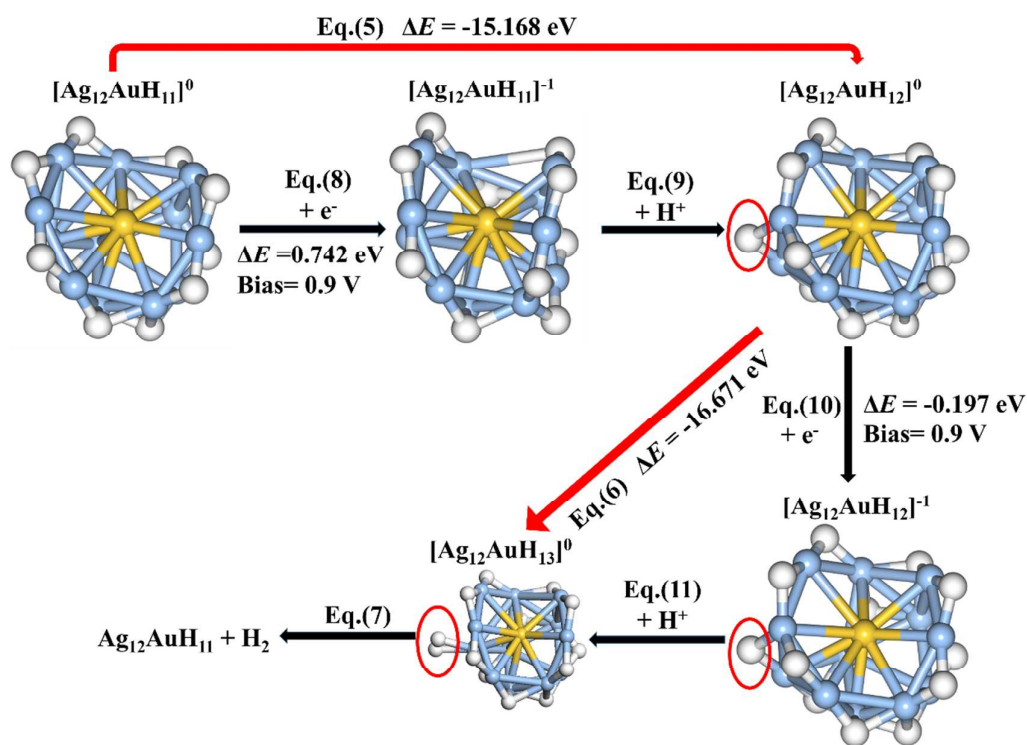


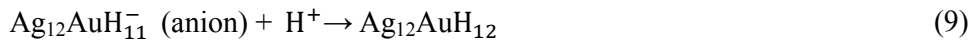
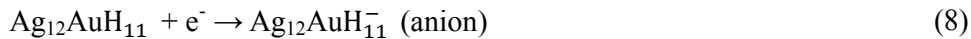
Figure 2. Schematic energy diagram illustrating the HER processes on the $\text{Ag}_{12}\text{AuH}_{11}$ catalyst via a super-saturation path; for Eq. 5 and 6, ΔE =Energy differences between two neutral clusters; for Eq. 8 and 10, ΔE = WF (work function of Pt electrode) – EA (electronic affinity) at -0.9V bias. Color coding as in Figure 1, with H atoms in white color.

The resulting ΔG for the first reaction-step of the HER process, Eq. (5), comes out to be 0.835 eV . We thus expect from a thermodynamic point of view that reaction (5) can occur spontaneously at a cathode bias of -0.835 V or larger which is very close to

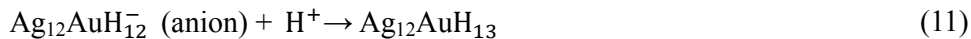
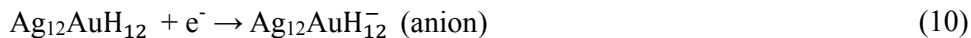
the bias typically used in HER devices, i.e. -0.9 V. The $\text{Ag}_{12}\text{AuH}_{11}$ cluster thus seems to realize a nearly ideal energetics, entailing an energy dissipation in the process of only 0.065 eV under typical conditions. To predict catalytic efficiency, we need to evaluate the free energy barrier associated with this reaction. To achieve this, we should in principle model the composite system: cluster+Pt-electrode+water-solvent. Modeling at the QM level such a large system is unfeasible using our computational resources. We can however model the cluster without the electrode, and we use both implicit-solvent (3.2.a) and explicit-solvent (3.2.b) models to simulate the surrounding water.

3.2.a Super-saturation path – implicit-solvent model

We take a simplified path to provide an estimate of the efficiency of the HER process, and decompose Eq.(5) into two successive steps, i.e., cluster electron affinity (EA) and hydronium attachment, as follows:



where Eq.(8) corresponds to the $\text{EA}(\text{Ag}_{12}\text{AuH}_{11})$ electron affinity or charging process, while Eq.(9) corresponds to the attachment of a hydronium ion to the $\text{Ag}_{12}\text{AuH}_{11}^-$ anion. The EA of $\text{Ag}_{12}\text{AuH}_{11}$ in water solution estimated using the Born formula Eq.(1) is 3.525 eV, thus charging of a cluster in close vicinity to a Pt hydrogen electrode at -0.9 V bias results in an energy penalty of 0.742 eV ($\Delta E = \text{WF}(\text{Pt})[\text{bias} = -0.9 \text{ V}] - \text{EA} = 4.267 - 3.525 = 0.742 \text{ eV}$), where $\text{WF}(\text{Pt})[\text{bias} = -0.9 \text{ V}]$ is the work function of the Pt electrode in water and at a bias of -0.9 V, as discussed in Section 2.1. Once the cluster is charged, the process of hydronium attachment onto it can be assimilated to those Grotthuss-like processes determining the anomalously high proton conductivity of water⁶⁶, and can be so expected to be fast. We note that the free energy barrier thus estimated considering two independent and successive steps for cluster charging and hydronium attachment clearly represents an upper bound to the real barrier, which will likely be smaller than this value as the hydronium cation approaching the cluster will polarize the system and favor electron transfer from the Pt electrode. Anyway, the present discussion shows that the barrier for reaction (5) is not larger than 0.74 eV at -0.9 V bias and standard conditions, corresponding to a reasonably efficient HER catalyst.



As for the second HER step, the reaction energy of Eq. (6) is -0.67 eV at zero bias, i.e., it is thermodynamically strongly favored even at zero bias. Moreover, at -0.9 V bias, the charging energy of $\text{Ag}_{12}\text{AuH}_{12}$ is also favored: $\Delta E = \text{WF}(\text{Pt})[\text{bias} = -0.9 \text{ V}] - \text{EA} = 4.267 - 4.464 = -0.197 \text{ eV}$, indicating that a $\text{Ag}_{12}\text{AuH}_{12}$ cluster in water in contact with a Pt electrode at -0.9 V bias spontaneously charges to an anionic form. The hydronium attachment to such cluster is therefore expected to be fast and has not been further investigated.

3.2.b Super-saturation path – explicit-solvent model

The estimates in Section 3.2.a are based on an implicit model for the solvent and on assuming the free energy of the (hydronium plus electron) pair equal to one-half of the free energy of gas-phase H_2 at zero bias, then properly shifting this quantity at a generic bias V [48,51-53]. Here we overcome the implicit solvent modeling via explicit-solvent AIMD simulations of the “ $\text{Ag}_{12}\text{AuH}_{11}^-$ (anion) + $\text{H}_3\text{O}^+ \rightarrow \text{Ag}_{12}\text{AuH}_{12}$ ” process to estimate the associated free-energy barrier. To this purpose, we start from AIMD runs at room temperature on the $\text{Ag}_{12}\text{AuH}_{11}$ neutral cluster surrounded by explicit water molecules (see Section 2 for computational details). We monitor the distance of closest approach of the H_2O molecule to the cluster, and select the snapshot in which one of the molecules achieve minimum distance, implying that the corresponding O atom is pointed toward one Ag atom of the cluster. We add a H^+ species to this water transforming into a hydronium cation: since we still impose the system to be globally neutral, this implies that the $\text{Ag}_{12}\text{AuH}_{11}$ cluster is negatively charged to compensate, thus forming a $[\text{Ag}_{12}\text{AuH}_{11}^- \text{ anion}/\text{H}_3\text{O}^+ \text{ hydronium}]$ close ionic pair. To equilibrate the system, we first relax via DFT the atoms of the $[\text{Ag}_{12}\text{AuH}_{11}^- \text{ anion}/\text{H}_3\text{O}^+ \text{ hydronium}]$ pair keeping the water molecules frozen, and then we conduct 10 psec AIMD simulation of the water keeping the ionic pair frozen: this represents the starting configuration of the hydronium attachment process – Eq.(9). The end configuration of this process is obtained by moving a H atom from hydronium to the cluster, thus obtaining a $[\text{Ag}_{12}\text{AuH}_{12} \text{ cluster}/\text{H}_2\text{O} \text{ water}]$ neutral pair, whose atoms are then relaxed via DFT keeping the water molecules frozen.

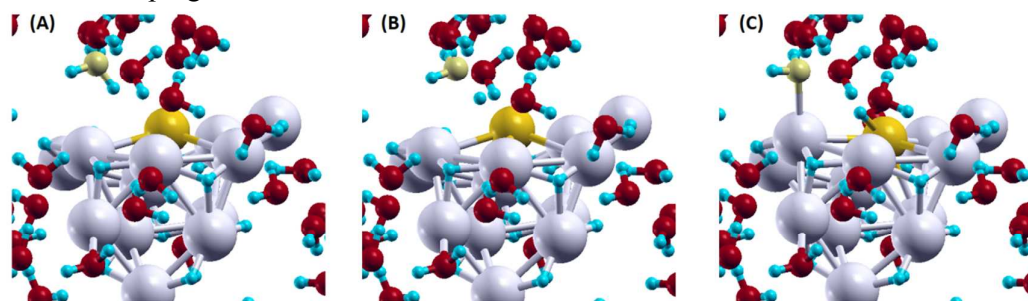


Figure 3. Schematic atomistic depiction of the NEB process transforming the $[\text{Ag}_{12}\text{AuH}_{11}^- \text{ anion}/\text{H}_3\text{O}^+ \text{ hydronium}]$ pair into a $[\text{Ag}_{12}\text{AuH}_{12} \text{ cluster}/\text{H}_2\text{O} \text{ water}]$ neutral pair, where panel (A) is the initial structure, panel (B) the saddle point, and panel (C) the final structure. Only few surrounding water molecules are visualized. Ag, Au, O, H atoms are represented by gray, yellow, red, and light blue spheres, respectively, with the O atom of the hydronium/water species in light green.

We finally evaluate the energy barrier between these two configurations by perform a NEB calculation in which the H_2O water molecules are kept frozen. An atomistic view of this process is illustrated in Figure 3. The energy barrier we thus estimate is 0.20 eV. The so-calculated barrier necessarily represents an upper bound to the real barrier, as the stabilization of the neutral species due to solvation is incomplete, water being frozen into a snapshot optimally adjusted to the charged $[\text{Ag}_{12}\text{AuH}_{11}^-/\text{H}_3\text{O}^+]$ configuration. To assess this effect quantitatively, an analogous DFT-relaxation+NEB simulation protocol was conducted in which the water molecules were still frozen, but adjusted to the neutral system: this alternative protocol gave a NEB barrier of 0.10 eV. We can therefore reasonably estimate the barrier for the hydronium attachment process – Eq.(9) – as 0.15 eV, which, summed to the previous value of 0.74 eV, finally produces a predicted overall HER free-energy barrier of 0.89

eV in the super-saturation régime. It should be mentioned that in this estimate we have neglected the barrier associated with the approach of the hydronium to the cluster anion surface. Finally, given the strong thermodynamic driving force for the second hydronium attachment process – Eq.(11), we have not performed AIMD simulations on the $\text{Ag}_{12}\text{AuH}_{12}^-$ cluster similar to those conducted on $\text{Ag}_{12}\text{AuH}_{11}^-$ to estimate the barrier to hydronium attachment which is expected to be negligible, i.e., we expect that reaction (6) occurs much more rapidly compared to reaction (5), which is thus the rate-determining step.

In conclusion, from the previous analysis we find that for HER on $\text{Ag}_{12}\text{AuH}_{11}$ the first Volmer-Heyrovsky step is rate-determining in the super-saturation régime, and the estimated free energy barriers do not exceed 0.89 eV as an upper bound. These findings make of Ag_{12}Au a potentially interesting system as a HER catalyst.

4. CONCLUSIONS

Hydrogen (H_2) production by electrochemical water splitting (via the HER) represents a promising alternative to fossil-fuel-based energy storage¹⁻⁷. Although the most popular HER electrocatalysts are based on platinum, its high cost and global scarcity have promoted efforts to develop alternative catalysts⁸⁻¹⁸. Here we propose Ag-Au subnanometer clusters as potentially favorable candidates in this context and illustrate such a proposal by investigating computationally the Ag_{12}Au nanoalloy as a model catalyst. In our approach, we first determine the resting state of the catalyst under realistic (standard) conditions, i.e., at high hydrogen coverage^{58, 59}, and then investigate the mechanistic steps according to the Volmer-Heyrovsky route via DFT and AIMD atomistic simulations including the effect of the bias and the effect of the water environment via both implicit and explicit models.

Our results indicate that the Ag_{12}Au cluster can act as a reasonably efficient HER electrocatalyst under realistic conditions. We find that the H-adsorption saturation level on this system is up to 11 hydrogen atoms, while further hydrogens undergo spontaneous H_2 evolution. The energetics of HER mechanistic steps seem favorable via a super-saturation path, with a nearly iso-energetic balance for the first Volmer-Heyrovsky step, which is also the rate-determining-step with an energy barrier estimated to be not larger than 0.89 eV, while the second Volmer-Heyrovsky step is largely favored thermodynamically, and should quickly convert $\text{Ag}_{12}\text{AuH}_{12}$ into $\text{Ag}_{12}\text{AuH}_{13}$, which we find then spontaneously evolves a H_2 molecule.

The proposed subnanometer catalysts, in analogy with previous experimental work^{29,30} in which very small clusters (including $\text{Ag}_{3,9,15}$ clusters on a carbon cathode for Li batteries) have been used under realistic electrochemical conditions, are also shown via AIMD simulations to possess some degree of robustness, with disaggregation barriers of the $\text{Ag}_{12}\text{AuH}_{11}$ free cluster at least > 0.25 eV (Section 3.1).

The reasons of the reasonable HER efficiency of the Ag_{12}Au catalysts is strictly connected to its ultra-nano form, and can be sought in the enhanced metal-hydrogen affinity when noble metals are shaped into subnanometer clusters, see e.g. Ref.⁶⁷, whereas larger, non-subnanometer particles are not expected to be active as HER catalysts without promotion from light²⁷, as hydrogen adsorption is too weak on these systems.

Interestingly, our analysis also suggests that a slight increase in the chemical affinity of the $\text{Ag}_{12}\text{AuH}_{11}$ cluster, i.e., of its affinity toward electrons and hydrogen species, could simultaneously decrease HER energy barriers and achieve a better

balance between first and second Volmer-Heyrovsky steps^{1, 8, 31}. This might be realized by introducing a third metal element which incidentally could also be beneficial in anchoring the cluster to the electrode: work is in progress to explore HER along these lines. The obtained mechanistic insight can thus be used to devise improved catalysts for experimental and computational testing. The present work thus suggests a promising avenue for deriving and rationally designing metal ultrananoclusters as potentially efficient and cost-effective electro-catalysts in the HER.

Acknowledgements

L.C. is grateful to the China Scholarship Council for a scholarship support that made this work possible during an internship at CNR-ICCOM. Support from CINECA supercomputing centre within the ISCRA programme is gratefully acknowledged, while the use of the Center for Nanoscale Materials, an Office of Science user facility, was supported by the U. S. Department of Energy, Office of Science, Office of Basic Energy Sciences, under Contract No. DE-AC02-06CH11357. D.C. gratefully acknowledges support from the National Natural Science Foundation of China (21576008, 91634116, 91334203).

REFERENCES

1. Z. W. Seh, J. Kibsgaard, C. F. Dickens, I. Chorkendorff, J. K. Norskov and T. F. Jaramillo, *Science*, 2017, **355**.
2. L. E. Doman, V. Arora, L. E. Singer, V. Zaretskaya, A. Jones, T. Huetteman, M. Bowman, N. Slater-Thompson, B. Hojjati, D. Peterson, P. Gross, P. Otis, M. Lynes and P. Lindstrom, *International Energy Outlook 2016*, U.S. Energy Information Administration 2016.
3. J. O. M. Bockris, *Energy: the solar - hydrogen alternative*, John Wiley and Sons, Inc., New York; None 1975.
4. J. Ohi, *J. Mater. Res.*, 2005, **20**, 3180-3187.
5. N. S. Lewis and D. G. Nocera, *Proc. Natl. Acad. Sci.*, 2006, **103**, 15729-15735.
6. A. Fortunelli, W. A. Goddard III, L. Sementa and G. Barcaro, *Nanoscale*, 2015, **7**, 4514-4521.
7. J. Wu and H. Yang, *Acc. Chem. Res.*, 2013, **46**, 1848-1857.
8. D. Strmcnik, P. P. Lopes, B. Genorio, V. R. Stamenkovic and N. M. Markovic, *Nano Energy*, 2016, **29**, 29-36.
9. H. Zhou, F. Yu, Y. Liu, J. Sun, Z. Zhu, R. He, J. Bao, W. A. Goddard, S. Chen and Z. Ren, *Energy Environ. Sci.*, 2017, **10**, 1487-1492.
10. A. Xie, N. Xuan, K. Ba and Z. Sun, *ACS Appl. Mater. Interfaces*, 2017, **9**, 4643-4648.
11. T. R. Hellstern, J. Kibsgaard, C. Tsai, D. W. Palm, L. A. King, F. Abild-Pedersen and T. F. Jaramillo, *ACS Catal.*, 2017, 7126-7130.
12. C. C. McCrory, S. Jung, I. M. Ferrer, S. M. Chatman, J. C. Peters and T. F. Jaramillo, *J.*

-
- Am. Chem. Soc.*, 2015, **137**, 4347-4357.
13. J. R. McKone, E. L. Warren, M. J. Bierman, S. W. Boettcher, B. S. Brunschwig, N. S. Lewis and H. B. Gray, *Energy Environ. Sci.*, 2011, **4**, 3573-3583.
 14. J. R. McKone, B. F. Sadtler, C. A. Werlang, N. S. Lewis and H. B. Gray, *ACS Catal.*, 2013, **3**, 166-169.
 15. M. G. Walter, E. L. Warren, J. R. McKone, S. W. Boettcher, E. A. S. Qixi Mi and N. S. Lewis, *Chem. Rev.*, 2010, **110**, 6446-6473.
 16. J. R. McKone, S. C. Marinescu, B. S. Brunschwig, J. R. Winkler and H. B. Gray, *Chem. Sci.*, 2014, **5**, 865-878.
 17. K. Kwak, W. Choi, Q. Tang, M. Kim, Y. Lee, D.-E. Jiang and D. Lee, *Nat. Commun.*, 2017, **8**, 14723.
 18. Y. Shi and B. Zhang, *Chem. Soc. Rev.*, 2016, **45**, 1529-1541.
 19. *Metal clusters and nanoalloys - From modeling to applications*, M. M. Mariscal, O. A. Oviedo and E. P. M. Leiva Eds., Springer Science & Business Media, 2012.
 20. G. Barcaro, A. Caro and A. Fortunelli, in *Springer Handbook of Nanomaterials*, ed. R. Vajtai, Springer Berlin Heidelberg, Berlin, Heidelberg, 2013, pp. 409-472.
 21. *Nanoalloys: From fundamentals to emergent applications*, F. Calvo Ed., Elsevier, Amsterdam, 2013.
 22. R. Ferrando, *Structure and Properties of Nanoalloys*, in *Frontiers of Nanoscience*, Elsevier, Amsterdam, 2016.
 23. Y. Attia and M. Samer, *Renew. Sust. Energ. Rev.*, 2017, **79**, 878-892.
 24. C. An, S. Wang, Y. Sun, Q. Zhang, J. Zhang, C. Wang and J. Fang, *J. Mater. Chem. A*,

-
- 2016, **4**, 4336-4352.
25. C. Gao, Y. Hu, M. Wang, M. Chi and Y. Yin, *J. Am. Chem. Soc.*, 2014, **136**, 7474-7479.
26. Y. A. Attia, D. Buceta, F. G. Requejo, L. J. Giovanetti and M. A. Lopez-Quintela, *Nanoscale*, 2015, **7**, 11273-11279.
27. J. Cui, Y. Li, L. Liu, L. Chen, J. Xu, J. Ma, G. Fang, E. Zhu, H. Wu, L. Zhao, L. Wang and Y. Huang, *Nano Lett.*, 2015, **15**, 6295-6301.
28. Y. A. Attia, D. Buceta, C. Blanco-Varela, M. B. Mohamed, G. Barone and M. A. López-Quintela, *J. Am. Chem. Soc.*, 2014, **136**, 1182-1185.
29. T. Chao, X. Luo, W. Chen, B. Jiang, J. Ge, Y. Lin, G. Wu, X. Wang, Y. Hu, Z. Zhuang, Y. Wu, X. Hong and Y. Li, *Angew. Chem. Int. Ed.*, 2017, **56**, 16047-16051.
30. J. Lu, L. Cheng, K. C. Lau, E. Tyo, X. Luo, J. Wen, D. Miller, R. S. Assary, H. H. Wang, P. Redfern, H. Wu, J. B. Park, Y. K. Sun, S. Vajda, K. Amine and L. A. Curtiss, *Nat. Commun.*, 2014, **5**, 4895.
31. Y. Zheng, Y. Jiao, M. Jaroniec and S. Z. Qiao, *Angew. Chem. Int. Ed.*, 2015, **54**, 52-65.
32. Paolo Giannozzi, Stefano Baroni, Nicola Bonini, Matteo Calandra, Roberto Car, Carlo Cavazzoni, Davide Ceresoli, Guido L. Chiarotti, Matteo Cococcioni, Ismaila Dabo, Andrea Dal Corso, Stefano Fabris, Guido Fratesi, Stefano de Gironcoli, Ralph Gebauer, Uwe Gerstmann, Christos Gougoussis, Anton Kokalj, Michele Lazzeri, Layla Martin-Samos, Nicola Marzari, Francesco Mauri, Riccardo Mazzarello, Stefano Paolini, Alfredo Pasquarello, Lorenzo Paulatto, Carlo Sbraccia, Sandro Scandolo, Gabriele

-
- Sclauzero, Ari P. Seitsonen, Alexander Smogunov, Paolo Umari and Renata M. Wentzcovitch, *J. Phys.: Condens. Matter*, 2009, **21**, 395502.
33. S. Grimme, J. Antony, S. Ehrlich and H. Krieg, *J. Chem. Phys.*, 2010, **132**, 154104.
34. John P. Perdew, Kieron Burke and M. Ernzerhof, *Phys. Rev. Lett.*, 1996, **77**, 3865-3868.
35. V. Barone, M. Casarin, D. Forrer, M. Pavone, M. Sambri and A. Vittadini, *J. Comput. Chem.*, 2009, **30**, 934-939.
36. S. Grimme, *J. Comput. Chem.*, 2006, **27**, 1787-1799.
37. R. Elber and M. Karplus, *Chem. Phys. Lett.*, 1987, **139**, 375-380.
38. G. Henkelman, B. P. Uberuaga and H. Jónsson, *J. Chem. Phys.*, 2000, **113**, 9901-9904.
39. G. Henkelman and H. Jónsson, *J. Chem. Phys.*, 2000, **113**, 9978-9985.
40. J. Hutter, M. Iannuzzi, F. Schiffmann and J. VandeVondele, *WIREs: Comput. Mol. Sci.*, 2014, **4**, 15-25.
41. Gerald Lippert, Jürg Hutter and M. Parrinello, *Theor. Chem. Acc.*, 1999, **103**, 124-140.
42. S. Goedecker, M. Teter and J. Hutter, *Phys. Rev. B*, 1996, **54**, 1703-1710.
43. J. VandeVondele and J. Hutter, *J. Chem. Phys.*, 2007, **127**, 114105.
44. M. Rambukwella, L. Sementa, A. Fortunelli and A. Dass, *J. Phys. Chem. C*, 2017, **121**, 14929-14935.
45. P. R. Nimmala, S. Theivendran, G. Barcaro, L. Sementa, C. Kumara, V. R. Jupally, E. Apra, M. Stener, A. Fortunelli and A. Dass, *J. Phys. Chem. Lett.*, 2015, **6**, 2134-2139.
46. J. D. Benck, T. R. Hellstern, J. Kibsgaard, P. Chakthranont and T. F. Jaramillo, *ACS*

-
- Catal.*, 2014, **4**, 3957-3971.
47. Y. Jiao, Y. Zheng, M. Jaroniec and S. Qiao, *Chem. Soc. Rev.*, 2015, **44**, 2060-2086.
48. E. Skulason, V. Tripkovic, M. E. Bjorketun, S. Gudmundsdottir, G. Karlberg, J. Rossmeisl, T. Bligaard, H. Jonsson and J. K. Nørskov, *J. Phys. Chem. C*, 2010, **114**, 18182-18197.
49. J. Greeley and M. Mavrikakis, *Nat. Mater.*, 2004, **3**, 810-815.
50. J. Greeley, T. F. Jaramillo, J. Bonde, I. B. Chorkendorff and J. K. Nørskov, *Nat. Mater.*, 2006, **5**, 909-913.
51. E. Skulason, G. S. Karlberg, J. Rossmeisl, T. Bligaard, J. Greeley, H. Jonsson and J. K. Nørskov, *Phys. Chem. Chem. Phys.*, 2007, **9**, 3241-3250.
52. J. Rossmeisl, J. K. Nørskov, C. D. Taylor, M. J. Janik and M. Neurock, *J. Phys. Chem. B*, 2006, **110**, 21833-21839.
53. J. K. Nørskov, J. Rossmeisl, A. Logadottir, L. Lindqvist, J. R. Kitchin, T. Bligaard and H. Jonsson, *J. Phys. Chem. B*, 2004, **108**, 17886-17892.
54. L. A. Kibler, *Chem. Phys. Chem.*, 2006, **7**, 985-991.
55. E. langenbach, A. Spitzer and H. Luth, *Surf. Sci.*, 1984, **147**, 179-190.
56. L. O. Paz-Borbon, R. L. Johnston, G. Barcaro and A. Fortunelli, *Eur. Phys. J. D*, 2009, **52**, 131-134.
57. M. Cerbelaud, R. Ferrando, G. Barcaro, A. Fortunelli, *Phys Chem Chem Phys.*, 2011, **13**, 10232-40.
58. F. R. Negreiros, E. Apra, G. Barcaro, L. Sementa, S. Vajda and A. Fortunelli, *Nanoscale*, 2012, **4**, 1208-1219.

-
59. F. R. Negreiros, G. Barcaro, L. Sementa and A. Fortunelli, *C. R. Chimie*, 2014, **17**, 625-633.
60. E. d. V. Gómez, S. Amaya-Roncancio, L. B. Avalor, D. H. Linares and M. C. Gimenez, *Appl. Surf. Sci.*, 2017, **420**, 1-8.
61. P. Ferrin, S. Kandoi, A. U. Nilekar and M. Mavrikakis, *Surf. Sci.*, 2012, **606**, 679-689.
62. M. Hu, D. P. Linder, M. Buongiorno Nardelli and A. Striolo, *J. Phys. Chem. C*, 2013, **117**, 15050-15060.
63. A. K. Gatin, M. V. Grishin, N. V. Dokhlikova, N. N. Kolchenko and B. R. Shub, *Doklady Phys. Chem.*, 2016, **470**, 125-128.
64. J. K. Nørskov, F. Abild-Pedersen, F. Studt and T. Bligaard, *Proc. Natl. Acad. Sci.*, 2011, **108**, 937-943.
65. C. Mager-Maury, G. Bonnard, C. Chizallet, P. Sautet and P. Raybaud, *ChemCatChem*, 2011, **3**, 200-207.
66. O. Markovitch, H. Chen, S. Izvekov, F. Paesani, G. A. Voth and N. Agmon, *J. Phys. Chem. B*, 2008, **112**, 9456-9466.
67. G. Barcaro, L. Sementa, F. R. Negreiros, and A. Fortunelli, *Computat. Theoret. Chem.*, 2013, **1021**, 222-228.

Atomistic view of hydronium (H_3O^+) attachment to a subnanometer $\text{Ag}_{12}\text{AuH}_{11}^-$ HER catalyst.

